Climate
of the Past

Supplement of

A cosmogenic nuclide-derived chronology of pre-Last Glacial Cycle glaciations during MIS 8 and MIS 6 in northern Patagonia

Tancrède P. M. Leger et al.

Correspondence to: Tancrède P. M. Leger (tancrede.leger@ed.ac.uk)

1 Rock sample preparation, wet chemistry and exposure-age calculations

1.1 SUERC cosmogenic isotopes analysis laboratory methodology

Thirteen samples were processed at the Scottish Universities Environmental Research Centre (SUERC) cosmogenic isotope analysis facility (Glasgow, Scotland) (main paper Table 1). Following rock sample crushing and sieving, the 125-250 μm and 250-500 μm grain fractions were cleaned and oven-dried to remove non-mineralic grains, prior to being magnetically separated. Non-magnetic fractions were recovered. To remove feldspar and mica minerals, the samples were treated with 1% *HF*, eucalyptus oil and a carbonated surfactant solution of water and dodecylamine to enable froth floatation (Herber, 1969). Non-floating quartz grains were recovered while floating minerals were stored. The samples were then etched in high-power ultrasonic baths a minimum of three times (24 h each) in 1000 ml of pure water, 40% *HF* and 68% *HNO$_3$* (150:2:1) to isolate the quartz grain cores, thus removing meteoric ^{10}*Be* (Kohl and Nishiizumi, 1992). A 0.4 g aliquot of the final quartz sample was dissolved and its purity tested for *Al*; *Be*; *Fe*; *Ca* and *Ti* by Inductively Coupled Plasma - Optical Emission Spectrometry. Samples containing higher-than-300 ppm *Al* concentrations were re-etched. Purified samples were dissolved in 40% *HF* and each sample and process blank were spiked with between 0.27 and 0.29 mg of ^{9}*Be,* using an in-house carrier solution obtained from phenakite (< 2 x10^{-15} ^{10}*Be/^{9}Be*). After dissolution, the *HF* was evaporated and replaced by *HCl*. The solutions were first passed through anion exchange chromatography columns to remove *Fe*. The *Fe*-free fractions were then evaporated and the *HCl* was replaced by dilute *H$_2$SO$_4$*. The sulphate solutions were then passed through cation exchange chromatography columns to remove *Ti* and *B*, and to isolate *Be* and *Al* fractions, eluted using *HCl* solutions. The *Be* and *Al* fractions were precipitated as hydroxides and oxidised at ~900 °C. Resulting *BeO* and *Al$_2$O$_3$* samples were mixed with *Nb* (1:6 ratio) and *Ag* (1:2 ratio), respectively, and pressed into copper cathodes for AMS measurements. ^{10}*Be/^{9}Be* and ^{26}*Al/^{27}Al* ratios were determined with a 5MV Tandem Pelletron (NEC Model 15SDH-2). All ^{10}*Be/^{9}Be* ratios were normalised to NIST SRM4325 with a nominal ^{10}*Be/^{9}Be* ratio of 2.79 x10^{-11} (Nishiizumi *et al*., 2007), corresponding to a ^{10}*Be* half-life of 1.36 Ma. Sample ^{10}*Be/^{9}Be* AMS measurement uncertainties ranged between 1.4% and 2.5%. Processed blank corrections for ^{10}*Be* concentrations ranged between 0.9% and 4.1% of the sample ^{10}*Be/^{9}Be* ratios. ^{26}*Al/^{27}Al* ratios were normalised to the Purdue Z92-0222 standard, with a nominal ^{26}*Al/^{27}Al* ratio of 4.11 x10^{-11}, equivalent to standardisation of ^{26}*Al* concentrations using the KNSTD standard (Nishiizumi, 2004). Processed blank corrections for ^{26}*Al* concentrations ranged between 0.2% and 0.4% of the sample ^{26}*Al/^{27}Al* ratios. The uncertainty of this correction is included in the stated standard uncertainties. The standard uncertainties also include between 3% and 11% for the uncertainty of stable ^{27}*Al* determination.

1.2 CEREGE LN₂C laboratory methodology

Five samples (RC20-12, 14, 16, 20, and 21) presenting low quartz yields were processed at the French National Laboratory for Cosmogenic Nuclides (LN₂C) of CEREGE, Aix-en-Provence, France (main paper Table 1). Following rock sample crushing and sieving, one to three treatments in *HCl*, *H₂SiF₆* and *HF* on a shaker table for 48 hours per treatment was performed to reduce/remove non-quartz minerals (inspired by Bourlès, 1988). Feldspar and other remaining non-quartz minerals were further reduced by magnetic separation after addition of magnetite powder. Pure quartz was obtained by repeated etching in a *HF* solution (*HF* 48%) diluted with ultrapure water (resistivity of 18.2 MΩ. cm⁻¹ at 25°C) for 24 hours in a heated ultrasonic bath, with a variable sample-to-acid ratio dependent on sample mass and mass conservation goals. At least 30% of pre-etching sample mass was dissolved, thus ensuring efficient removal of atmospheric ^{10}Be (Kohl and Nishiizumi, 1992). The purified quartz samples were dissolved in concentrated *HF* (48%) and each sample and one process blank were spiked with between 0.439 and 0.456 mg of ^9Be, in the form of an in-house carrier solution made from phenakite. After dissolution, the *HF* was evaporated and the solid residue was dissolved in *HCl* (10.2 mol L⁻¹) followed by *Be(OH)₂* precipitation at pH ~9 through the addition of *NH₃,* and re-dissolution in *HCl* (10.2 mol L⁻¹). The solutions were first passed through anion exchange chromatography columns to remove *Fe*, *Ti* and *Mn*. After another evaporation and *Be(OH)₂* precipitation step, *HCl* of lower concentration (1 mol L⁻¹) was added to dissolve the *Be* prior to passing the solution through cation exchange chromatography columns to isolate *Be* from *B* and *Al*. The *Be* fractions were then precipitated again as hydroxides (pH ~9), prior to dissolution in 200 μL of *HNO₃* (65%) and oxidation for 1 hour at ~700 °C. The resulting *BeO* samples were mixed with *Nb* powder (1:1 ratio) and pressed into nickel cathodes for AMS measurements at the ASTER AMS facility. $^{10}Be/^9Be$ ratio measurements are based on the in-house standard *STD-11* (equivalent to NIST SRM4325 and the 07KNSTD standards) with a $^{10}Be/^9Be$ ratio of (1.191 ± 0.013) x10⁻¹¹ (Braucher *et al*., 2015) and a ^{10}Be half-life of (1.387 ± 0.0012) x10⁶ years (Chmeleff *et al*., 2010; Korschinek *et al*., 2010). Analytical uncertainties include ASTER counting statistics and stability (the latter being ~0.5%; Arnold *et al*., 2010) and machine blank correction. $^{10}Be/^9Be$ AMS measurement uncertainties ranged between 2.4% and 3.5%. Process blank corrections ranged between 0.6% and 1.5% of calculated sample ^{10}Be atoms.

1.3 University of Edinburgh Cosmogenic Nuclide Laboratory methodology

Five samples (RHS09, 10, 12, 13, 15) were processed for wet chemistry at the University of Edinburgh Cosmogenic Nuclide Laboratory (main paper Table 1). The ~1 kg samples were crushed whole and sieved to isolate the 250-500 μm grain fractions. One to three treatments in *HCl* and *H₂SiF₆* on a shaker table for up to seven days per treatment was performed to reduce/remove non-quartz minerals (Bourlès, 1988). Pure quartz was obtained by repeated etching in a 2% *HF* and 1% *HNO₃* solution for 24 hours in a heated ultrasonic bath, with a sample to acid ratio of about 12 g L^{-1}. At least three etches were then performed to remove atmospheric ^{10}Be. Between 0.248 and 0.250 mg of ^{9}Be carrier was added to quartz separates prior to dissolution in concentrated HF (48%). The dissolved samples were fumed in *HClO₄* and passed through anion exchange chromatography columns to remove *Fe* and other contaminants. Precipitation to remove *Ti* was followed by separation of *Be* from *Al* by cation exchange chromatography. These were precipitated and fumed in *HClO₄* to reduce Boron levels. Hydroxide gels were rinsed with ultra-pure water, dried, fired in a furnace, mixed with *Nb* and pressed into cathodes for AMS measurements at SUERC (section 1.1.).

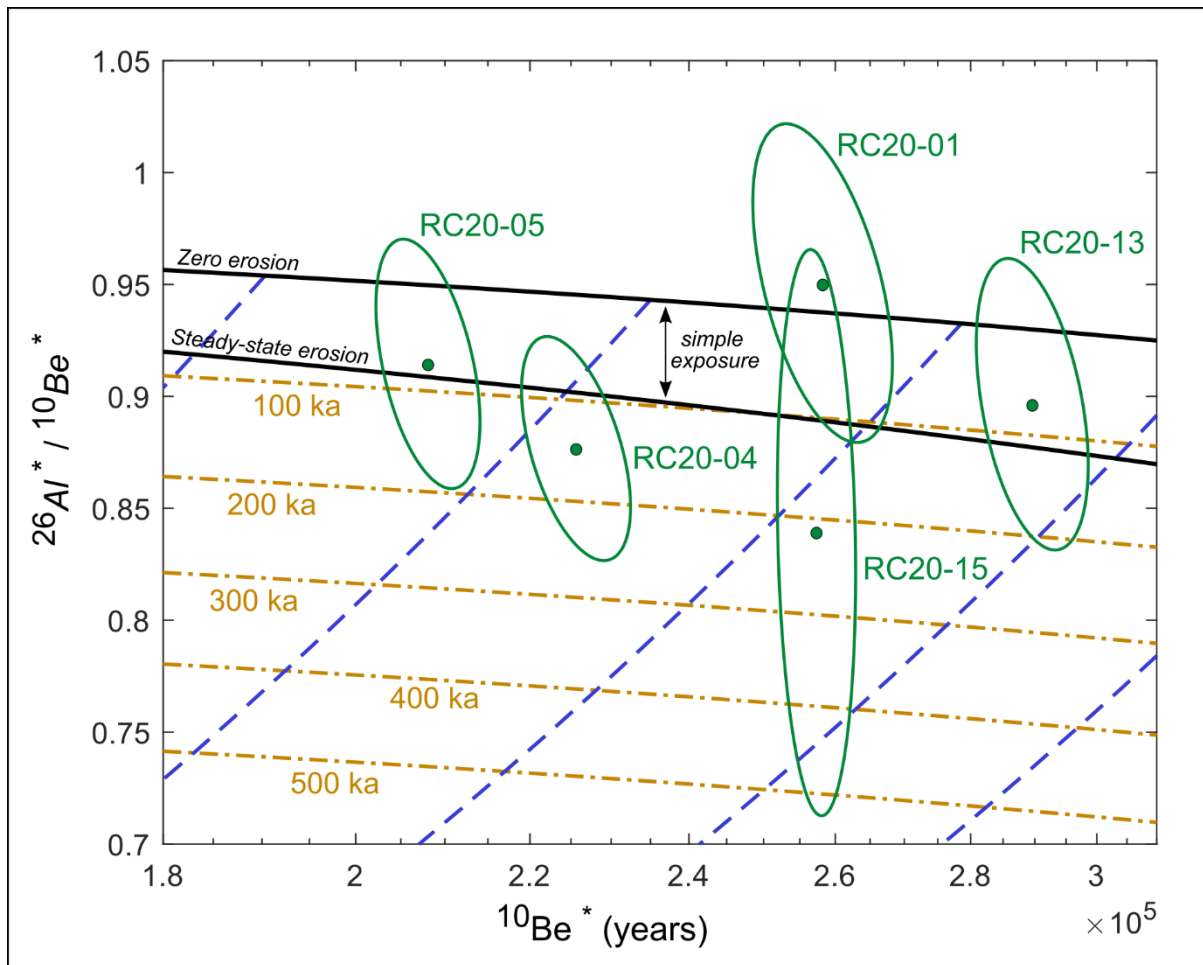## 2 ^{10}Be and ^{26}Al concentrations ratio analysis

Figure S1. Two-isotope diagram of the five samples for which both ^{10}Be and ^{26}Al concentrations in quartz were determined. This plot was adapted from plots produced using the iceTEA tools for exposure ages Matlab© code (Jones *et al.*, 2019). The diagram features ^{10}Be and ^{26}Al concentrations normalised at SLHL by the global production rate of Borchers *et al.* (2016). The thick black lines highlight the simple exposure region. Sample point means and uncertainty ellipses (1σ uncertainties) are symbolised in green. Isochrones indicate lines of equal burial time (orange dot-dashed lines) and equal exposure time (blue dashed lines). The data shows that within 1σ analytical uncertainties (green ellipses), all sample nuclide concentrations fall inside the simple exposure region, thus suggesting all samples underwent a simple, single exposure and erosion history (Dunai, 2010). If samples fall below the simple exposure region within analytical uncertainties, $^{26}Al/^{10}Be$ ratios would instead indicate that samples experienced periods of burial and thus a complex exposure history. RC20-04,05 are moraine boulders from the RC II margin, RC20-01 is an ice-moulded bedrock surface sample located between the RC I and RC II margins, and RC20-13,15 are outwash surface cobbles from the RC I margin (main paper Table 1 and 2).

3 Sample location maps

3.1 RC II moraine-outwash complex samples & RC I-II ice-moulded bedrock sample
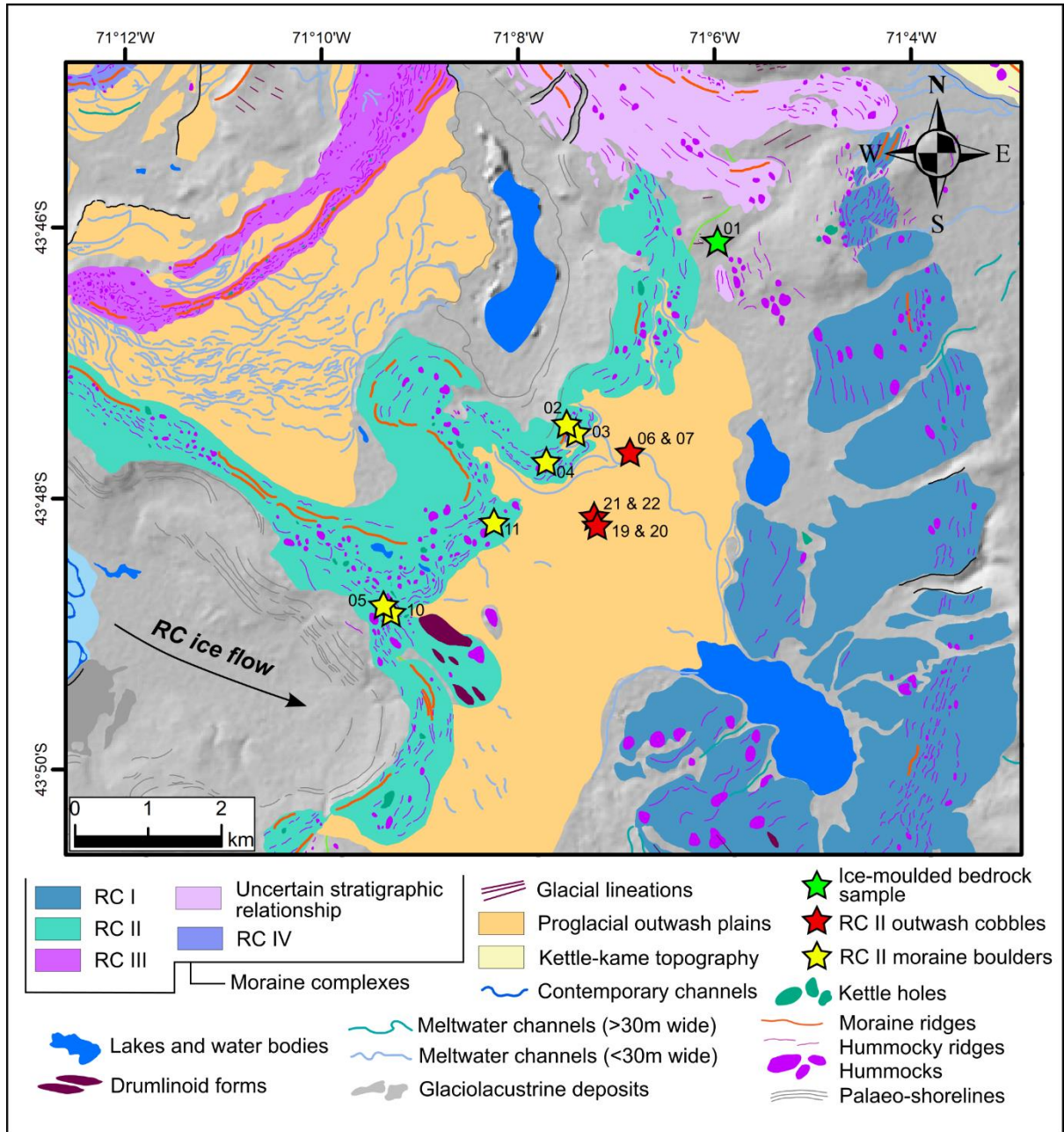

Figure S2. Glacial geomorphological mapping (hillshade from ALOS WORLD 3D 30m DEM) focused on sampling locations of the RC II moraine-outwash complex. The locations of RC II outwash surface cobbles and RC II moraine boulders sampled for TCN exposure dating are denoted by red and yellow stars, respectively.
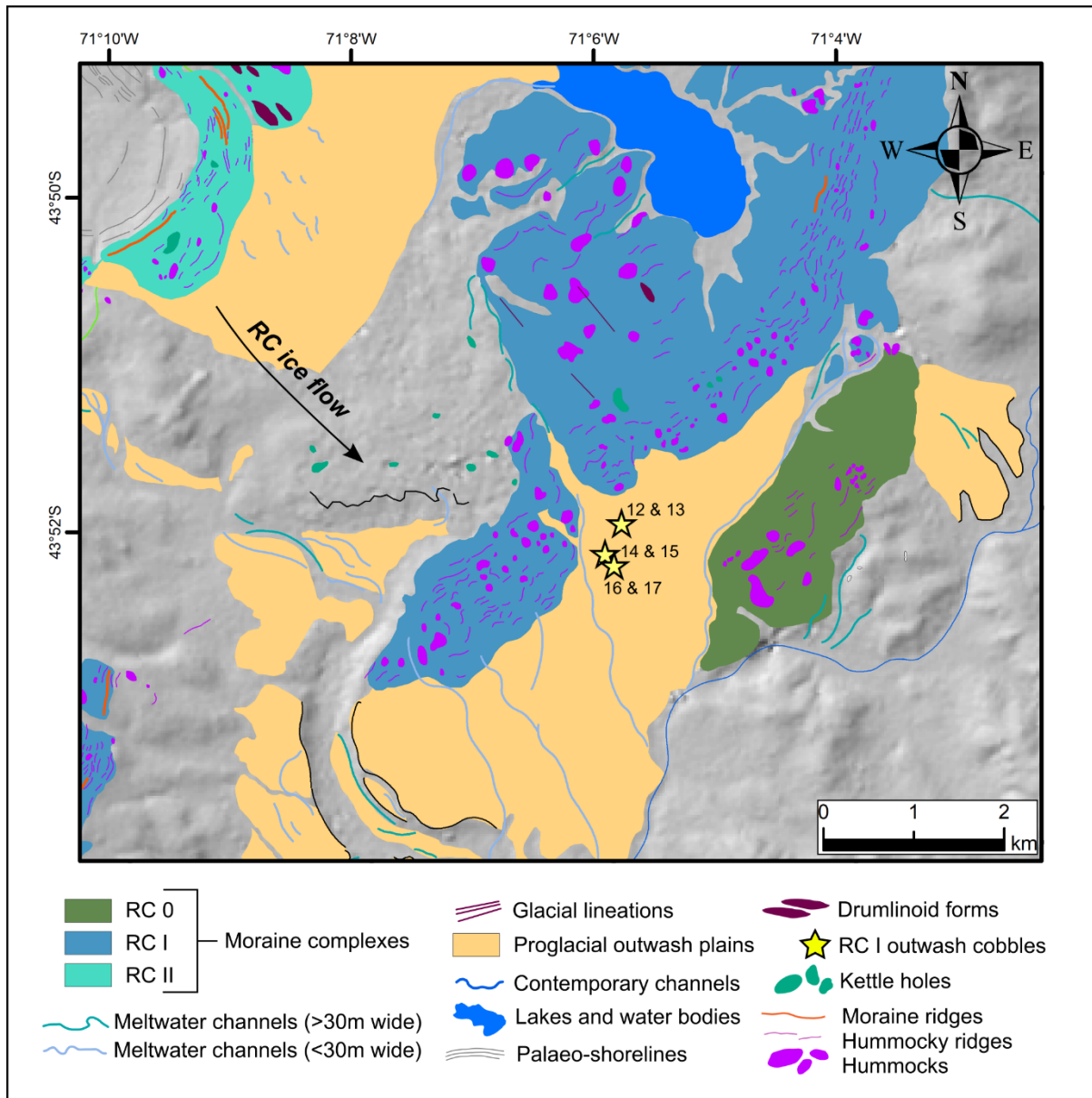
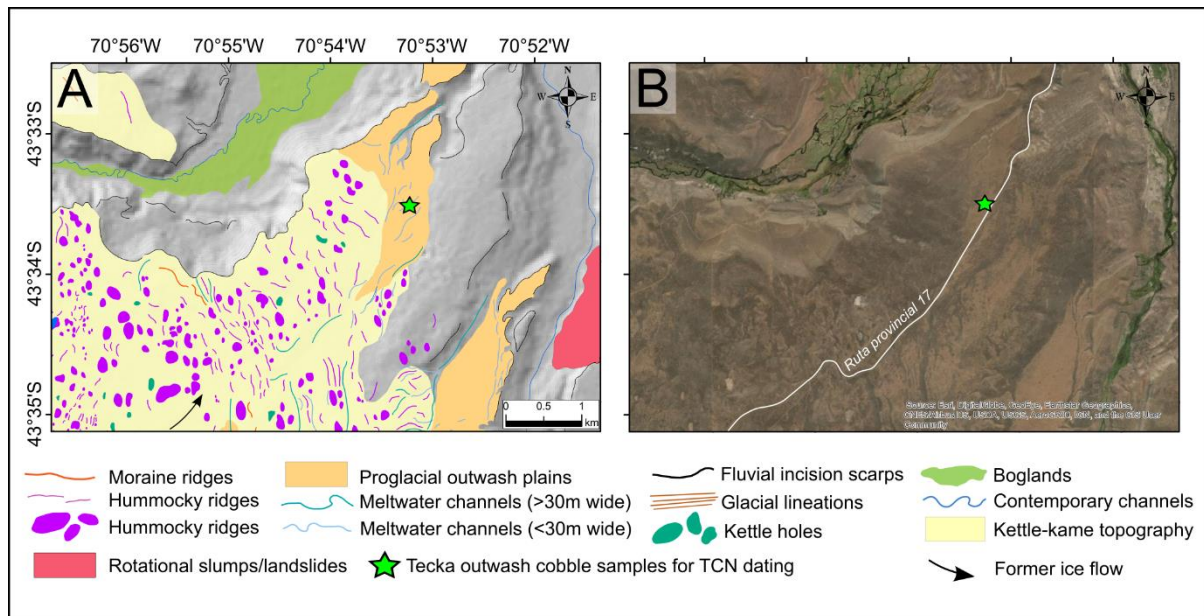## 3.2 RC I moraine-outwash complex samples

Figure S3. Glacial geomorphological mapping (hillshade from ALOS WORLD 3D 30m DEM) focused on the sampling location of the RC I moraine-outwash complex. The locations of RC I outwash surface cobbles sampled for TCN exposure dating are denoted by yellow stars.

3.3 Tecka / RC 0 outwash samples

Figure S4. A) Glacial geomorphological mapping (hillshade from ALOS WORLD 3D 30m DEM) and **B**) Satellite imagery (ESRI[TM], DigitalGlobe) comparison of the outermost belt of ice-contact glaciogenic kettle-kame deposit located to the east of the Río Huemul valley, and also termed the Tecka Drift (Haller *et al*., 2003). The northeastern edge of this deposit makes way to a proglacial outwash plain that was sampled for TCN exposure dating of surface cobbles (n=5, green star). We interpret this deposit as stratigraphically corresponding to the outermost moraine belt preserved in the Río Corcovado valley, here termed the RC 0 moraine.

4 Sample photographs

RC20-01

RC20-02

RC20-03

RC20-04

RC20-05

RC20-10

RC20-11

RC20-06

RC20-07

RC20-19

RC20-22

RC20-20

RC20-21

RC20-12

RC20-14

RC20-13

RC20-15

RC20-16

5 Method: estimating potential impact of outwash-cobble exhumation on exposure-age scatter

To estimate the possible impact of cobble exhumation through a soil horizon (*e.g.* via cryoturbation) on post-depositional exposure-age scatter and landform formation age underestimation, we conducted simulations of constant-rate cobble exhumation through soil columns of various thicknesses. Because the spallation-dominated production of cosmogenic ^{10}Be in quartz is reduced with depth below surface due to cosmic-ray attenuation (Gosse & Phillips, 2001), taking into account sample cover since deposition will result in older exposure ages than calculated if assuming a constant exposure history. Our approach is based on the assumption that, for depths <25 cm and relative to a simple exposure history, ^{10}Be concentration attenuation for a cobble exhumed at a constant-rate through a given soil depth is approximately equivalent to the ^{10}Be concentration attenuation for a cobble that is constantly buried below that given depth / 2. This mathematical simplification is based on the negligible curvature (relationship considered close to linear) of the theoretical cosmic-ray attenuation trajectory at such shallow depths, especially given the relatively low density (~1.3 g cm^{-3}) of soil material. We use the IceTEA tools for exposure ages[1] (Jones *et al*., 2019) to calculate new sample shielding factors after taking into account a correction for constant sample cover by soil, prior to re-calculating exposure ages using the new shielding factor and the online calculator formerly known as the CRONUS-Earth online calculator version 3 (Balco *et al*., 2008). The time-averaged surface shielding factor (*Ss*) is calculated from:

$$Ss = St \, exp\left(-\frac{Zcover \; Pcover}{\Delta s}\right) \tag{1}$$

Where *St* is the field-measured topographic shielding factor, *Zcover* is the given depth of sample cover below surface (cm), *Pcover* is the given average cover-material density (g cm^{-3}) and Δs is the attenuation length (g cm^{-2}), calculated from sample location (Sato *et al*., 2008). Throughout our simulations, we use an average dry mineral soil density of 1.3 g cm^{-3}. Note that a more site-specific value could be obtained by conducting soil moisture-content measurements in the field. We conducted a series of calculations using variable soil depths until the sample population (*e.g.* RC II outwash cobbles) mean exposure age post-simulation was similar to the population's oldest cobble's original exposure age. This is considered a better minimum age-estimate for the timing of landform deposition due to post-depositional age scatter causing young apparent ages. For these exposure ages to match, the estimated soil depth through which all cobbles hypothetically exhumed at a constant rate was ~12 cm and ~24 cm (equivalent to constant burial below ~6 and ~12 cm-thick soil covers) for the Tecka outwash and the RC II outwash cobble sample populations, respectively. Resulting mean exposure ages were increased by 5.7% and 10.8% for the Tecka and RC II outwash samples, respectively.

---

[1] *http://ice-tea.org/en/tools/correct-surface-cover/*

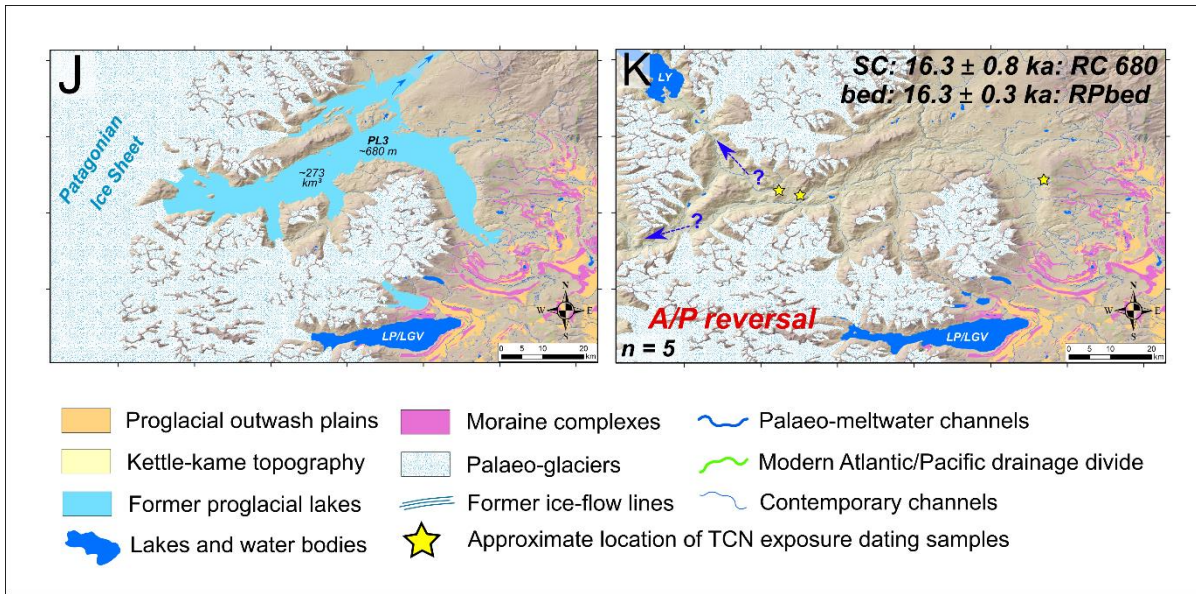# 6 Studied PIS outlet-glacier reconstruction: summary figure
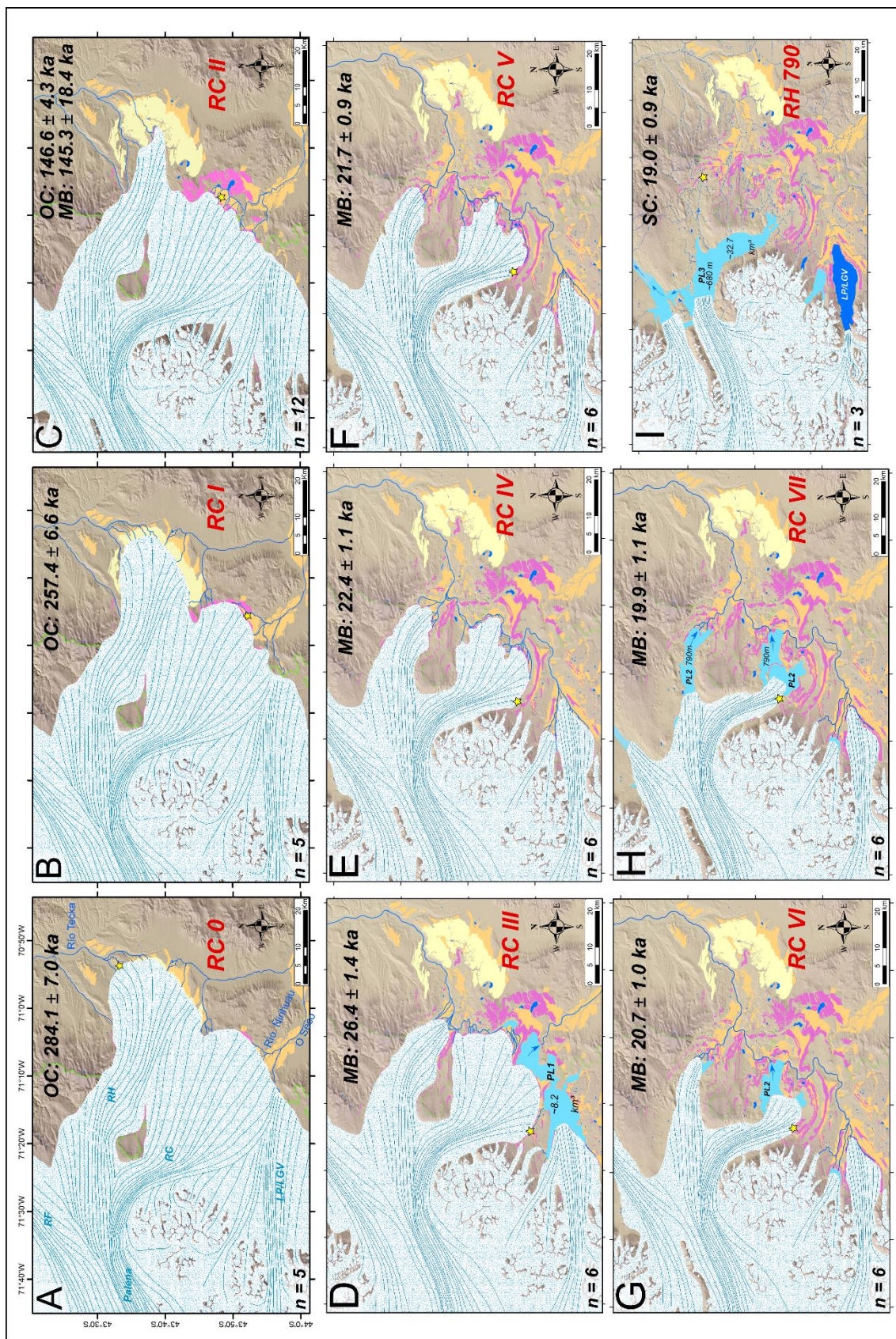
Figure S5. Palaeoglacial and palaeolake reconstructions for the RC, RH, RF and Lago Palena/General Vintter valleys, for advances/stillstands and deglacial events interpreted in this investigation (**A-C**) as well as companion publications (Leger *et al*., 2020, 2021a,). Ice-sheet and mountain glacier models were digitised manually in ArcGIS. Except when delineated by confidently mapped moraine limits (*e.g.* the RC, RH and LP/LGV moraine sequences), the geographical location of ice margins are inferred from topography. "*OC*", "*MB*", "*SC*", and "*bed*" denote the type of rock samples used for TCN exposure dating of the represented event, and stand for "*outwash cobbles*", "*moraine boulders*", "*shoreline cobbles*", and "*bedrock*", respectively. Yellow stars indicate the approximate sample locations for TCN exposure dating of each represented event, while each panel features the number of exposure ages produced (n = x) towards the bottom left-hand corner. (**A-H**): Ice extents associated with the RC 0 to RC VII moraine complexes. This includes the formation of glaciolacustrine phase one and two (here termed PL1 and PL2, respectively). There are no previously published numerical chronologies in the RH, RF and LP/LGV valleys. The relative ice extent in those neighbouring valleys is thus inferred based on our RC chronology and cross-valley comparisons of moraine numbers, preservation and morphostratigraphy. Hence, these inferences yield some uncertainties. (**I**): Reconstruction of the opening of the RF valley scenario and the subsequent RC proglacial lake lowering to 680 m (dated with shoreline surface cobbles from the RH$_{790}$ shoreline), marking the onset of glaciolacsutrine phase 3 (here denoted: PL3), according to our geomorphic interpretation. (**J**): Reconstruction of the westward retreat of the RP outlet glacier towards the core of the Andes and the associated expansion of the 680 m proglacial lake. (**K**): Reconstruction of the onset of PIS disintegration, enabling ice-dam collapse and the Pacific-directed, final drainage of the 680 m proglacial lake (PL3). Proglacial lake volume estimates were computed from DEM data (AW3D30). Panel **K** question marks relate to the uncertainty regarding the former drainage pathway(s) employed during the local Atlantic/Pacific drainage reversal event. Location of ice fronts for panels **I**, **J**, **K** are hypothetical as not correlated to specific geomorphic limits, but are aimed at representing specific events/scenarios.

Supplementary materials – specific references

Arnold, M., Merchel, S., Bourlès, D.L., Braucher, R., Benedetti, L., Finkel, R.C., Aumaître, G., Gottdang, A., Klein, M, 2010, The French accelerator mass spectrometry facility ASTER: improved performance and developments: Nuclear Instruments and Methods in Physics Research Section B: Beam Interactions with Materials and Atoms, v 268(11-12), p 1954-1959, doi: https://doi.org/10.1016/j.nimb.2010.02.107.

Bourlès, D. Etude de la géochimies de l'isotope cosmogénique 10Be et de son isotope stable 9Be en milieu océanique. Application à la datation des sédiments marins (1988). Ph.D. thesis, Univ. Paris XI

Braucher, R., Guillou, V., Bourlès, D.L., Arnold, M., Aumaître, G., Keddadouche, K., and Nottoli, E., 2015, Preparation of ASTER in-house 10Be/9Be standard solutions: Nuclear Instruments and Methods in Physics Research Section B: Beam Interactions with Materials and Atoms, v. 361, p. 335-340, doi: https://doi.org/10.1016/j.nimb.2015.06.012.

Chmeleff, J., von Blanckenburg, F., Kossert, K., and Jakob, D., 2010, Determination of the 10Be half-life by multicollector ICP-MS and liquid scintillation counting: Nuclear Instruments and Methods in Physics Research Section B: Beam Interactions with Materials and Atoms, v. 268(2), p. 192-199, doi: https://doi.org/10.1016/j.nimb.2009.09.012.

Kohl, C. P., & Nishiizumi, K. (1992). Chemical isolation of quartz for measurement of in-situ-produced cosmogenic nuclides. Geochimica et Cosmochimica Acta, v. 56(9), p. 3583-3587, doi: https://doi.org/10.1016/0016-7037(92)90401-4.

Korschinek, G., Bergmaier, A., Faestermann, T., Gerstmann, U. C., Knie, K., Rugel, G., Wallner, A., Dillmann, I., Dollinger, G., Lierse von Gostomski, Ch., Kossert, K., Maiti, M., Poutivtsev, M., Remmert, A., 2010, A new value for the half-life of 10Be by heavy-ion elastic recoil detection and liquid scintillation counting: Nuclear Instruments and Methods in Physics Research Section B: Beam Interactions with Materials and Atoms, v. 268(2), p. 187-191, doi: https://doi.org/10.1016/j.nimb.2009.09.020.

Nishiizumi, K., 2004, Preparation of 26Al AMS standards: Nuclear Instruments and Methods in Physics Research Section B: Beam Interactions with Materials and Atoms, v. 223, p. 388-392, doi: https://doi.org/10.1016/j.nimb.2004.04.075.

Nishiizumi, K., Imamura, M., Caffee, M.W., Southon, J.R., Finkel, R.C., and McAninch, J., 2007, Absolute calibration of 10Be AMS standards: Nuclear Instruments and Methods in Physics Research Section B: Beam Interactions with Materials and Atoms, v. 258(2), p. 403-413, doi: https://doi.org/10.1016/j.nimb.2007.01.297.

Sato, T., Yasuda, H., Niita, K., Endo, A., and Sihver, L., 2008, Development of PARMA: PHITS-based analytical radiation model in the atmosphere: Radiation research, v. 170(2), p. 244-259, doi, https://doi.org/10.1667/RR1094.1.